Inorganic Chemistry

Article

pubs.acs.org/IC

Electrochemical Behavior of α_1/α_2-$[Fe(H_2O)P_2W_{17}O_{61}]^{7-}$ Isomers in Solution: Experimental and DFT Studies

Neus Vilà,[†] Pablo A. Aparicio,[‡] Francis Sécheresse,[†] Josep M. Poblet,[‡] Xavier López,[‡,*] and Israël M. Mbomekallé*,[†]

[†]Université de Versailles St. Quentin, Institut Lavoisier de Versailles, UMR8180 CNRS, Versailles, F-78035, France

[‡]Departament de Química Física i Inorgànica, Universitat Rovira i Virgili, Marcel·lí Domingo s/n, 43007 Tarragona, Spain

Supporting Information

ABSTRACT: The unusual redox behavior displayed by the two isomers of the Wells–Dawson phosphotungstate anion $[Fe(H_2O)P_2W_{17}O_{61}]^{7-}$ is presented. The electrochemical measurements have been performed in aqueous media at different pH values from 0.5 up to 8.0. The cyclic voltammetry has also been carried out in organic media to get additional experimental data to establish the effect of the protonation on the redox properties of both isomers. At high pH values (pH ≥ 6) or in an organic medium, the reduction of the Fe center is easier in the case of the alpha-1 isomer, whereas for the alpha-2 isomer such reduction takes place at more negative potentials, as expected. In contrast, at lower pH values (pH ≤ 5), an inversion of this trend is observed, and the reduction of the Fe center becomes easier for the alpha-2 isomer compared to the alpha-1. We were able to highlight the influence of the pH and the pK_a of the electrolyte on POM-based redox potentials given the pK_a of the latter. A complementary theoretical study has also been performed to explain the experimental data obtained. In this sense, the results obtained from the DFT study are in good agreement with the experimental data mentioned above and have provided additional information for the electrochemical behavior of both isomers according to their different molecular orbital energies. We have also shown the influence of protonation state of the iron derivative on the relative reduction potentials of both isomers.

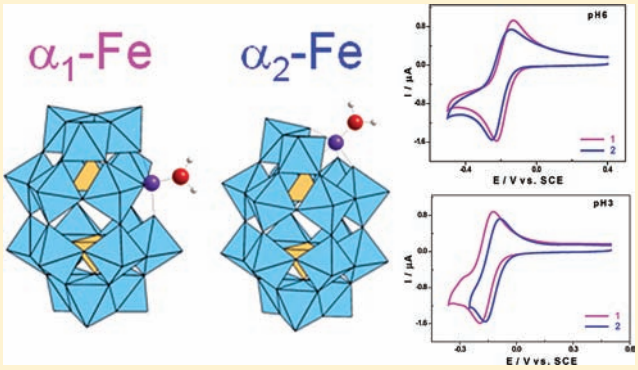

INTRODUCTION

Polyoxometalates (POMs) are known to behave as electron pumps; they may act as donors or as acceptors in reversible electron transfer processes. Generally, these processes take place simultaneously with proton exchange. Understanding of mechanisms that govern these electron (and proton) transfers and the characterization of the resulting species has become a main subject in POM science. The contributions include, among others, (1) the pioneering work of Souchay, Hervé, and co-workers[1−4] (2) and those of Pope and co-workers, who during the 1960s and 1970s, launched the basis for the electrochemistry of POMs.[5−9] Later, in the early 1990s, much more work devoted to the electrochemistry and electrocatalytic properties of POMs emerged.[10−13] Among remarkable contributions, the work of Keita and Nadjo should be highlighted, since they have irrefutably developed, promoted, and popularized the electrochemistry of POMs. Thus, electrochemical techniques have become an invaluable and crucial tool for the characterization of POMs, and they have usually been employed as models for the study and description of electron transfer processes and electrocatalytic mechanisms.[10,12,14,15] However, the extensive attention given to the redox properties of POMs has revealed many singular and unexpected behaviors that electrochemistry alone cannot explain. More recently, the introduction of DFT calculations has led to a better understanding of the properties of POMs.[16−21] On the basis of these encouraging results, we decided to combine electrochemistry and DFT calculations for systematical reinvestigation of the redox properties of POMs. Other techniques (NMR, EPR...) are sometimes needed to achieve a better understanding of the electronic properties of POMs as molecules or as materials. For example, very recently, we showed that within a given family of Keggin anions carrying the same electrical charge, apparent potential values decrease with the size of the central heteroatom.[22] The results and conclusion are of great importance because they complete the experimental rule established by Pope and Varga in 1966, which predicts that redox potentials of Keggin-type anions are a linear function of their overall charge.[5] The present study focuses on the redox behavior in solution of the two isomers, alpha-1 and alpha-2, of

Received: January 13, 2012
Published: May 15, 2012

   dx.doi.org/10.1021/ic300090f | Inorg. Chem. 2012, 51, 6129–6138

the Wells–Dawson phosphotungstate anion $[Fe(H_2O)P_2W_{17}O_{61}]^{7-}$ (Figure 1).

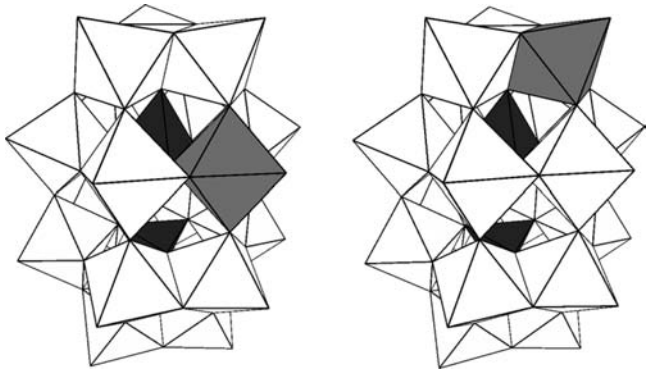

Figure 1. Idealized structure of α_1-$[Fe(H_2O)P_2W_{17}O_{61}]^{7-}$ (left) and α_2-$[Fe(H_2O)P_2W_{17}O_{61}]^{7-}$ (right) derivatives.

A former study conducted in aqueous solution by Keita et al.[23] has shown that, in aqueous solution and at very low pH values, the first redox process attributed to Fe^{3+}/Fe^{2+} reduction and the following one attributed to the reduction of the tungsten framework merged into a single three-electron wave for isomer α_1-$[Fe(H_2O)P_2W_{17}O_{61}]^{7-}$. Under the same experimental conditions, they remain separated for the isomer α_2-$[Fe(H_2O)P_2W_{17}O_{61}]^{7-}$, i.e., a first one-electron wave followed by a second two-electron wave. Another noteworthy observation is that, throughout the pH domain explored in that study (0.16–3.00), Fe^{3+}/Fe^{2+} reduction is easier in the case of α_2-$[Fe(H_2O)P_2W_{17}O_{61}]^{7-}$ than in the case of α_1-$[Fe(H_2O)P_2W_{17}O_{61}]^{7-}$. This result seems to contradict the electrochemical behavior observed with other metal-substituted Dawson-type tungstodiphosphates, such as $[MOP_2W_{17}O_{61}]^{x-}$ (with M = V or Mo), in which the reduction of the substituted metal cation, M^{n+}, is always easier for the alpha-1 isomer than for the alpha-2 isomer, at the pH where the species are stable.[24−29] The aim of the present work is to explain this particular behavior through a study of the redox properties of both compounds in aqueous and nonaqueous solutions and by means of DFT calculations.

EXPERIMENTAL SECTION

General Methods and Materials. Pure water obtained by passing water through a RiOs 8 unit followed by a Millipore-Q Academic purification set was used throughout. All reagents were of high-purity grade and were used as purchased without further purification. Pure samples of K_7-α_1-$[Fe(H_2O)P_2W_{17}O_{61}]\cdot 19H_2O$ (**1**) and K_7-α_2-$[Fe(H_2O)P_2W_{17}O_{61}]\cdot 19H_2O$ (**2**) were obtained by following a synthetic procedure previously reported.[30] Purity was confirmed by IR and cyclic voltammetry. The IR spectra were recorded with KBr pellets on a Nicolet Magna IR Spectrometer 550 spectrophotometer.

Electrochemical data were obtained using an EG&G 273 A driven by a PC with the M270 software. A one-compartment cell with a standard three-electrode configuration was used for cyclic voltammetry experiments. The composition of the various media was as follows: (1) for an aqueous medium, 0.2 M Na_2SO_4 + H_2SO_4 for pH 0.5–4, 0.4 M CH_3COONa + CH_3COOH for pH 4–6, and 0.4 M NaH_2PO_4 + 0.2 M Na_2HPO_4 + H_3PO_4 for pH 3–8; (2) for an organic medium, 0.1 M $LiClO_4$ in CH_3CN.

The polyanion concentration was 5×10^{-4} M. Prior to each experiment, solutions were deaerated thoroughly for at least 30 min with pure Ar. A positive pressure of this gas was maintained during subsequent work. All cyclic voltammograms were recorded at a scan rate of 10 mV s^{-1} unless otherwise stated. All experiments were performed at room temperature, which is controlled and fixed for the lab at 20 °C. The reference electrode was a saturated calomel electrode (SCE) and the counter electrode, a platinum gauze of large surface area; both electrodes separated from the bulk electrolyte solution via fritted compartments filled with the same electrolyte. The working electrode was a 3 mm o.d. glassy carbon disk (GC, Le Carbone de Lorraine, France). The pretreatment of this electrode before each experiment, adapted from the procedure of Keita and Nadjo,[31] was as follows: (1) Fine polishing was perfromed using diamond pastes (DP Diamond-Struers) of decreasing grain size (15 min with a grain size of 6 μm, 15 min with a grain size of 3 μm, and 30 min with a grain size of 1 μm). (2) The electrode then underwent two successive ultrasonic washings in ethanol and in Millipore water (or distilled acetonitrile when working in nonaqueous media), respectively, at 5 min each. Results were very reproducible from one experiment to another, and slight variations observed over successive runs are attributed to the uncertainty associated with the detection limit of our equipment (potentiostat, hardware, and software) and not to working electrode pretreatment nor to possible variations in temperature.

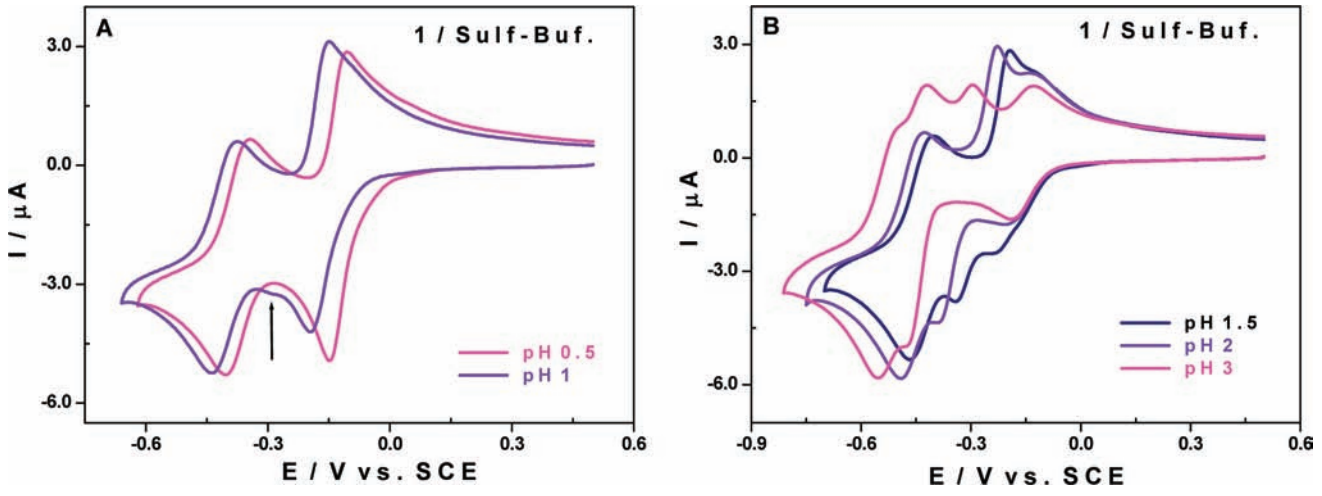

Figure 2. Cyclic voltammograms of **1** at different pH values. Polyoxometalate concentration, 0.5 mM; scan rate, 10 mV s^{-1}; working electrode, glassy carbon; reference electrode, SCE. (A) pH 0.50 (red line) and pH 1.00 (purple line). (B) pH 1.50 (black line), pH 2.00 (purple line), and pH 3.00 (red line).

dx.doi.org/10.1021/ic300090f | Inorg. Chem. 2012, 51, 6129–6138

COMPUTATIONAL DETAILS

The DFT calculations were carried out with the Gaussian 09 suite of programs.[32] Our calculations were performed using the B3LYP hybrid functional[33] with the 6-31G basis set for H and O atoms and the standard double-ζ basis set with Los Alamos National Laboratory pseudopotentials[34] (LANL2DZ) for W, Fe, and P atoms. All of the calculations include the *polarizable continuum model*[35] (PCM) to account for the solvent effects of water. The solute cavity was created using a scaled van der Waals surface and a grid of five points per Å^2. Atomic radii correspond to the Universal Force Field parameters. We applied the spin-unrestricted formalism to electronically open-shell molecules.

RESULTS AND DISCUSSION

The aim of the present work is to describe, understand, and rationalize the influence of protonation on the electrochemical behavior associated with the reduction of Fe(III) centers within alpha-1 and alpha-2 isomers of the Wells–Dawson compound $[Fe(H_2O)P_2W_{17}O_{61}]^{7-}$. To this purpose, cyclic voltammograms of both compounds **1** and **2** were recorded in several aqueous media (with the pH varying from 0.50 to 8.00) and in CH_3CN + 0.1 M $LiClO_4$. As shown in Figure SI-1A and Figure 2, a cyclic voltammogram of **1** recorded at pH 0.50 displays a first reversible three-electron wave located at −0.15 V vs SCE. Two additional two-electron voltammetric signals are observed at more negative potentials, −0.40 V and −0.70 V vs SCE. It should be highlighted that, at this pH value, the iron based reduction process takes place at the same potential as the first two-electron wave attributed to the W framework, resulting in a unique three-electron quasi-reversible wave (E_{pc} = −0.15 V and E_{pa} = −0.10 V vs SCE). A controlled potential electrolysis of this solution (pH 0.5) was performed at −0.15 V vs SCE. Consumption of 2.9 ± 0.1 mol of electron per 1 mol of **1** confirmed that, as previously mentioned,[23] both reduction processes (Fe^{3+} and W framework) are included in the first voltammetric signal. This wave undergoes significant changes when increasing pH: (1) As expected, a shift of the cathodic wave toward more negative potentials is observed. (2) This shift is accompanied with a gradual splitting starting at pH 1. (3) Concomitantly, the peak reduction current I_{pc} drops rapidly. At pH 3, two totally independent redox processes are evidenced, the first one located at E_{pc} = −0.19 V vs SCE is attributed to the one-electron reversible reduction of the Fe^{3+} center within **1**, and the second at more negative potentials, E_{pc} = −0.47 V vs SCE, is attributed to the first two-electron reduction of the W framework. The partial or complete merging of those two waves has been observed and well-described by Keita and co-workers, who have combined spectroscopic and electrochemical techniques to achieve a perfect understanding of this uncommon behavior.[23]

The electrochemical behavior of **2** is quite different compared to that of **1** under the same experimental conditions. For the entire medium tested in this study, the Fe^{3+}-based cathodic wave is observed separately from the W reduction process (see Supporting Information, SI). Furthermore, $E_{pc}(Fe^{3+})$ moves more rapidly toward negative potentials when increasing the pH for isomer **2** compared to **1**. Indeed, as summarized in Table SI-1, between pH 0.50 and pH 8.00, the average shift of $E_{pc}(Fe^{3+})$ is equal to 52 mV per pH unit. This is in accordance with the theoretical value of 59 mV per pH unit obtained from the Nernst equation. Meanwhile, for compound **1**, between pH 3.00 and pH 8.00 (pH domain where the Fe^{3+} wave is observed separately from first W wave), the $E_{pc}(Fe^{3+})$ shift observed is almost 3 times lower than that observed for **2**, i.e. 16 mV per pH unit ($\Delta E_{pc}(Fe^{3+})_{pH8-0.5}$ = 390 mV for **2** and $\Delta E_{pc}(Fe^{3+})_{pH8-3}$ = 80 mV for **1**). This narrow variation observed for the reduction of Fe^{3+} within **1** compared to **2** highlights the different acid–base properties of the two isomers. Indeed, Contant et al. showed that **1** is more basic than **2**, and they have determined the pk_a values of both complexes (pk_a(**1**) = 7.55; pk_a(**2**) = 5.85).[30] Many studies focused on the influence of pH on the electrochemical properties of POMs have proved that POM based redox processes at the working electrode are generally coupled to the proton exchange reaction through either an electrochemical–chemical (EC) or an electrochemical–chemical–electrochemical (ECE) mechanism. This proton-coupled electron transfer (PCET) will depend both on the composition of the electrolyte (pH and pk_a) and on the acid–base properties of the POM molecule (pk_a).

Combined pH and Electrolyte Influence. To carry out a rigorous study based on the pH and electrolyte influence on Fe^{3+} and W redox waves, one must proceed under experimental conditions where both waves can be observed separately; i.e., the splitting between Fe^{3+} and the first W waves is complete. As described and discussed above, this situation is observed for compound **2** in the whole pH domain explored here (0.5–8.0), while that for **1** is only observed starting at pH ≥ 3. Another coercion will be the electrolyte choice that should cover a pH domain where its buffer power remains non-negligible.

1. Sulfate Buffer (0.2 M Na_2SO_4 + H_2SO_4): pH 1–4. For compound **1**, the discussion on its electrochemical behavior will therefore be restricted to pH 3 and 4. Given its pk_a value (pk_a = 7.55), **1** is always in its protonated form α_1-$[HFe^{III}(OH_2)P_2W_{17}O_{61}]^{6-}$, within this pH range. Concerning the electrolyte, SO_4^{2-} is the predominant species within this pH interval {pK_a(HSO_4^-/SO_4^{2-}) = 1.9}, and its buffering capacity is rather limited. The reduction of Fe^{3+} takes place without consumption of any proton; i.e., it is pH independent and can be summarized as follows:

$$\alpha_1\text{-}[HFe^{III}(OH_2)P_2W_{17}O_{61}]^{6-} + e \rightleftharpoons \alpha_1\text{-}[HFe^{II}(OH_2)P_2W_{17}O_{61}]^{7-} \quad (1)$$

However, the following reduction steps (W reduction) are coupled with a transfer of protons and are obviously pH dependent (see Figure 3 and Table 1). For example, the second bielectronic reduction can be summarized as follows:

$$\alpha_1\text{-}[HFe^{II}(OH_2)P_2W_{17}O_{61}]^{7-} + 2e + 2H^+ \rightarrow \alpha_1\text{-}H_2[HFe^{II}(OH_2)P_2W_{17}O_{61}]^{7-} \quad (2)$$

In fact, the formal anionic POM charge has become very important, −7, and the addition of supplementary electrons will be compensated by the simultaneous addition of protons. This process can be described as an EC or ECE mechanism. In conclusion, between pH 3 and 4, the reduction of Fe^{3+} within **1** is pH independent, while W reduction depends on the pH (see Figure 3 and Table 1).

Regarding the electrochemical behavior of **2**, the Fe^{3+} reduction wave stands apart from W reduction wave at all pH values explored in this electrolyte (0.2 M Na_2SO_4 + H_2SO_4/pH 0.5–4). However, it is worth considering two distinct pH domains on the basis of the pk_a of the acid–base couple HSO_4^-/SO_4^{2-}. (1) pH ≤ 2, where HSO_4^- is predominant, and (2) pH > 2, where SO_4^{2-} is predominant.

dx.doi.org/10.1021/ic300090f | *Inorg. Chem.* 2012, 51, 6129–6138

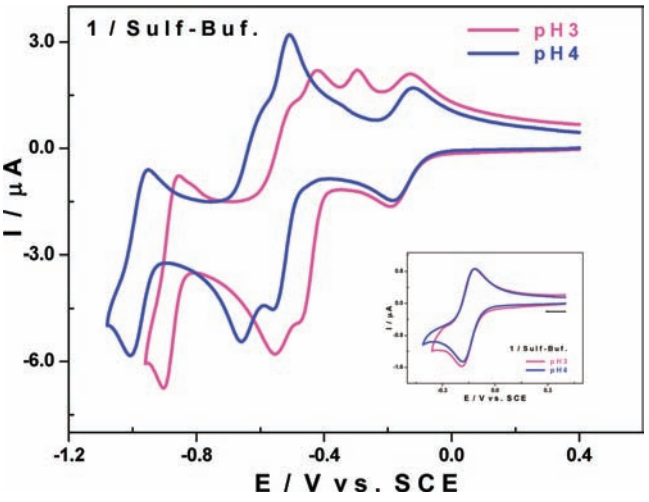

Figure 3. Cyclic voltammograms of **1** at pH 3 (red line) and pH 4 (blue line) in 0.2 M Na_2SO_4 + H_2SO_4. Polyoxometalate concentration, 0.5 mM; scan rate, 10 mV s^{-1}; working electrode, glassy carbon; reference electrode, SCE. Inset, CVs restricted to the Fe^{3+} wave.

Table 1. Peak Reduction Potential Values, E_{pc}, for Fe^{3+} Redox Process and First Three W^{6+} Redox Processes for 1 in 0.2 M Na_2SO_4 + H_2SO_4 at pH 3 and 4[a]

1	E_{pc} ($Fe^{3+/2+}$)	E_{pc} (W_1)	E_{pc} (W_2)	E_{pc} (W_3)
pH 3	−0.19	−0.47	−0.55	−0.90
pH 4	−0.18	−0.56	−0.66	−1.01

[a]Potentials are quoted against SCE reference electrode. Scan rate, 10 mV·s^{-1}; working electrode, glassy carbon.

Nevertheless, in any case, **2** will exist in its protonated form α_2-$[HFe^{III}(OH_2)P_2W_{17}O_{61}]^{6-}$ (pk_a = 5.85).

In the first interval (pH ≤ 2), the combined effect of strong acidity and prevalence of the acidic species HSO_4^- will favor a PCET process for both Fe^{3+} and W reductions. Both processes will be pH dependent (see Figure 4) and can be summarized as follows:

$$\alpha_2\text{-}[HFe^{III}(OH_2)P_2W_{17}O_{61}]^{6-} + e + H^+ \rightleftharpoons \alpha_2\text{-}H[HFe^{II}(OH_2)P_2W_{17}O_{61}]^{6-} \quad (3)$$

$$\alpha_2\text{-}H[HFe^{II}(OH_2)P_2W_{17}O_{61}]^{6-} + 2e + 2H^+ \rightleftharpoons \alpha_2\text{-}H_3[HFe^{II}(OH_2)P_2W_{17}O_{61}]^{6-} \quad (4)$$

The shift of the Fe^{3+} wave will continue up to pH 3 with an average shift of 64 mV per pH unit. This value is very close to the expected theoretical value of 59 mV according to the Nernst equation when one-electron and proton transfers are coupled.

Between pH 3 and 4, **2** will show exactly the same electrochemical behavior as described above for **1**; i.e., the Fe^{3+} wave is no more pH dependent while W redox steps show all of the characteristics of PCET processes (see Figure 5 and Table 2 below).

$$\alpha_2\text{-}[HFe^{III}(OH_2)P_2W_{17}O_{61}]^{6-} + e \rightleftharpoons \alpha_2\text{-}[HFe^{II}(OH_2)P_2W_{17}O_{61}]^{7-} \quad (5)$$

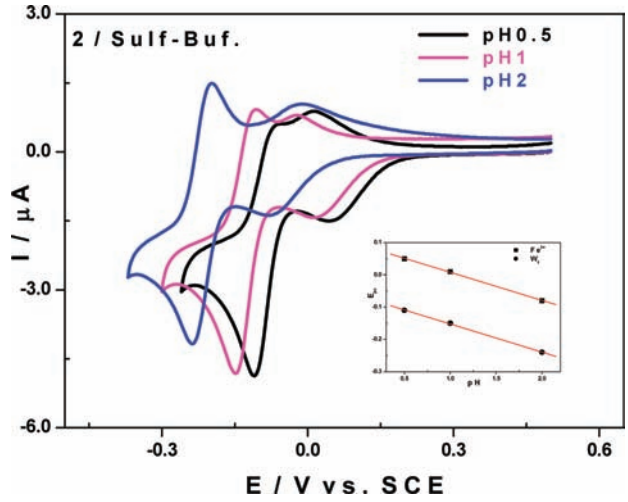

Figure 4. Cyclic voltammograms of **2** in 0.2 M Na_2SO_4 + H_2SO_4 at pH 0.5 (black line), pH 1 (red line), and pH 2 (blue line). Polyoxometalate concentration, 0.5 mM; scan rate, 10 mV s^{-1}; working electrode, glassy carbon; reference electrode, SCE. Inset, E_{pc}, peak reduction potential values for Fe^{3+} (squares) and W_1 (circles), as a function of pH.

$$\alpha_2\text{-}[HFe^{II}(OH_2)P_2W_{17}O_{61}]^{7-} + 2e + 2H^+ \rightleftharpoons \alpha_2\text{-}H_2[HFe^{II}(OH_2)P_2W_{17}O_{61}]^{7-} \quad (6)$$

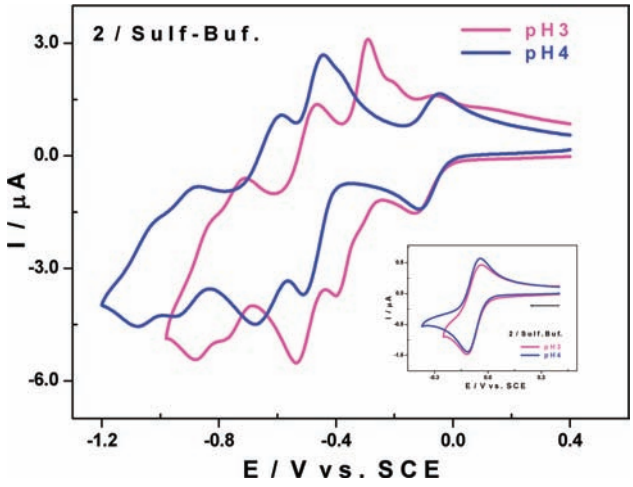

Figure 5. Cyclic voltammograms of **2** at pH 3 (red line) and pH 4 (blue line) in 0.2 M Na_2SO_4 + H_2SO_4. Polyoxometalate concentration, 0.5 mM; scan rate, 10 mV s^{-1}; working electrode, glassy carbon; reference electrode, SCE. Inset, CVs restricted to the Fe^{3+} wave.

Table 2. Peak Reduction Potential Values, E_{pc}, for Fe^{3+} Redox Process and First Three W^{6+} Redox Processes for 2 in 0.2 M Na_2SO_4 + H_2SO_4 in the Range of pH 0.5 to 4[a]

2	E_{pc} ($Fe^{3+/2+}$)	E_{pc} (W_1)	E_{pc} (W_2)	E_{pc} (W_3)
pH 0.5	+0.05	−0.11	−0.36	−0.68
pH 1	+0.01	−0.15	−0.39	−0.75
pH 2	−0.08	−0.24	−0.47	−0.72; −0.83
pH 3	−0.11	−0.39	−0.54	−0.78; −0.88
pH 4	−0.11	−0.58	−0.67	−0.95; −1.07

[a]Potentials are quoted against SCE reference electrode. Scan rate, 10 mV·s^{-1}; working electrode, glassy carbon.

dx.doi.org/10.1021/ic300090f | Inorg. Chem. 2012, 51, 6129−6138

2. Acetate Buffer: 0.4 M $NaCH_3COO$ + CH_3COOH. The pH range explored in an acetate buffer varies from pH 4 to 6 {pK_a (CH_3COOH/CH_3COO^-) = 4.7}. In this pH interval, **1** is protonated, and as expected, its electrochemical behavior is the same as observed in a sulfate buffer from pH 3 to 4 (see Figure 6 and Table 3 below). Equations 1 and 2 are still very illustrative of the redox processes occurring between the working electrode and the POM.

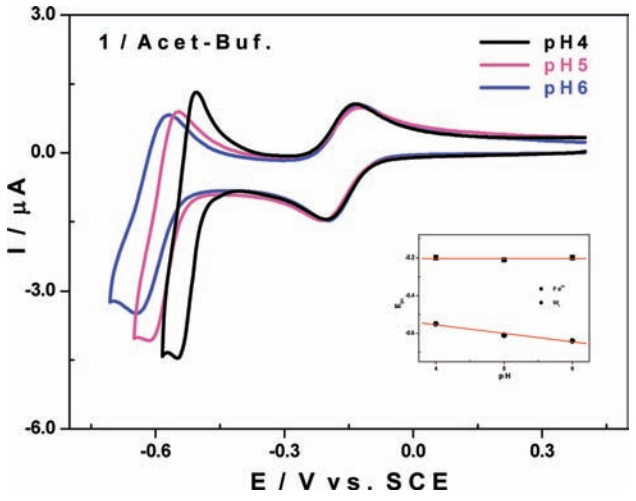

Figure 6. Cyclic voltammograms of **1** in 0.4 M $NaCH_3COO$ + CH_3COOH at pH 4 (black line), pH 5 (red line), and pH 6 (blue line). Polyoxometalate concentration 0.5 mM; scan rate 10 mV s^{-1}; working electrode, glassy carbon; reference electrode, SCE. Inset, E_{pc}, peak reduction potential values for Fe^{3+} (squares) and W_1 (circles), as a function of pH.

Table 3. Peak Reduction Potential Values, E_{pc}, for Fe^{3+} Redox Process and First Three W^{6+} Redox Processes for 1 and 2 in 0.4 M $NaCH_3COO$ + CH_3COOH in the Range of pH 4 to 6[a]

		E_{pc} ($Fe^{3+/2+}$)	E_{pc} (W_1)	E_{pc} (W_2)	E_{pc} (W_3)
1	pH 4	−0.20	−0.55	−0.63	−0.96
	pH 5	−0.21	−0.61	−0.72	−1.04
	pH 6	−0.20	−0.64	−0.78	−1.09
2	pH 4	−0.17	−0.48	−0.59	−0.87
	pH 5	−0.18	−0.55	−0.67	−0.92
	pH 6	−0.17	−0.60	−0.73	−0.99

[a]Potentials are quoted against SCE reference electrode. Scan rate, 10 mV·s^{-1}; working electrode, glassy carbon.

The same redox behavior is observed for **2**, although its acid−base behavior differs from that of **1** in this pH domain (Figure 7). At pH 4 and 5, **2** should be in its protonated form (pk_a = 5.85), and redox processes will be in good agreement with eqs 3 and 4. At pH 6, according to its pk_a value, **2** is no more protonated, but the effect of PCET process will balance the absence of protonation and apparent redox potentials, $E^{\circ\prime}$, for both reactions (reduction of protonated **2** without H^+ transfer—pH 4 and 5—and reduction of nonprotonated **2** with H^+ transfer—pH 6) have almost the same value (−0.14 V and −0.13 V vs SCE respectively).

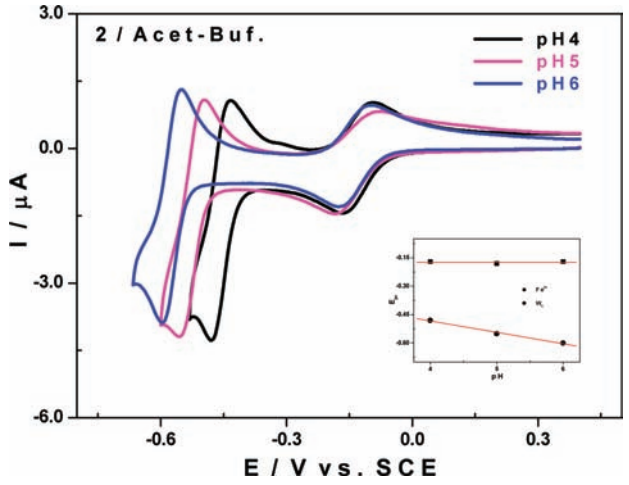

Figure 7. Cyclic voltammograms of **2** in 0.4 M $NaCH_3COO$ + CH_3COOH at pH 4 (black line), pH 5 (red line), and pH 6 (blue line). Polyoxometalate concentration, 0.5 mM; scan rate, 10 mV s^{-1}; working electrode, glassy carbon; reference electrode, SCE. Inset, E_{pc}, peak reduction potential values for Fe^{3+} (squares) and W_1 (circles), as a function of pH.

$$\alpha_2\text{-}[HFe^{III}(OH_2)P_2W_{17}O_{61}]^{6-} + e \rightleftharpoons \alpha_2\text{-}[HFe^{II}(OH_2)P_2W_{17}O_{61}]^{5-}, \quad E^{\circ\prime} = -0.14\ V$$

$$\alpha_2\text{-}[Fe^{III}(OH_2)P_2W_{17}O_{61}]^{6-} + e + H^+ \rightleftharpoons \alpha_2\text{-}H[Fe^{II}(OH_2)P_2W_{17}O_{61}]^{6-}, \quad E^{\circ\prime} = -0.13\ V$$

It is worth noting that in this medium, whatever the pH, Fe^{3+} within **2** is easier to reduce than within **1**.

3. Phosphate Buffer: 0.4 M NaH_2PO_4 + 0.2 M Na_2HPO_4 + H_3PO_4. The study will be very interesting in this medium because the prevalence of one species, $H_2PO_4^-$, covers almost the whole range of pH explored here {pK_{a1}($H_3PO_4/H_2PO_4^-$) = 2.1; pK_{a2}($H_2PO_4^-/HPO_4^{2-}$) = 7.2; pK_{a3}(HPO_4^{2-}/PO_4^{3-}) = 12.3}. In addition, $H_2PO_4^-$ has an amphoteric behavior, i.e., can either behave as an acid or as a base according to the acid−base properties of the compound with which it reacts.

From pH 3 to pH 5.5, **1** and **2** display different electrochemical behaviors, although both isomers are in their protonated forms. $E_{pc}(Fe^{3+})$ is restricted to a narrow interval (between −0.19 V and −0.21 V vs SCE) for **1**, while for **2** the shift is observed in a wider interval (−0.17 V to −0.24 V vs SCE). It seems that the effect of pH on Fe^{3+} reduction is more pronounced for **2** (28 mV/pH) than for **1** (8 mV/pH).

At pH 6 and higher, the basic form of **2** prevails (pk_a = 5.85); in addition, H^+ concentration becomes much lower. It should then be reasonable to conclude that both protonation and the pH effect are negligible. Even so, we still observe a significant shift of E_{pc} toward more negative potentials (45 mV/pH between pH 6 and 8). This fact can be explained according to the amphoteric nature of $H_2PO_4^-$, previously pointed out, which acts as the source of protons in this case making the reduction of Fe^{3+} still pH dependent.

Theoretically, **1** can still be protonated up to pH 7.5; the pH influence will then be very limited, and especially if we consider that, above pH 7.2, the predominant species in our electrolyte is

dx.doi.org/10.1021/ic300090f | Inorg. Chem. 2012, 51, 6129−6138

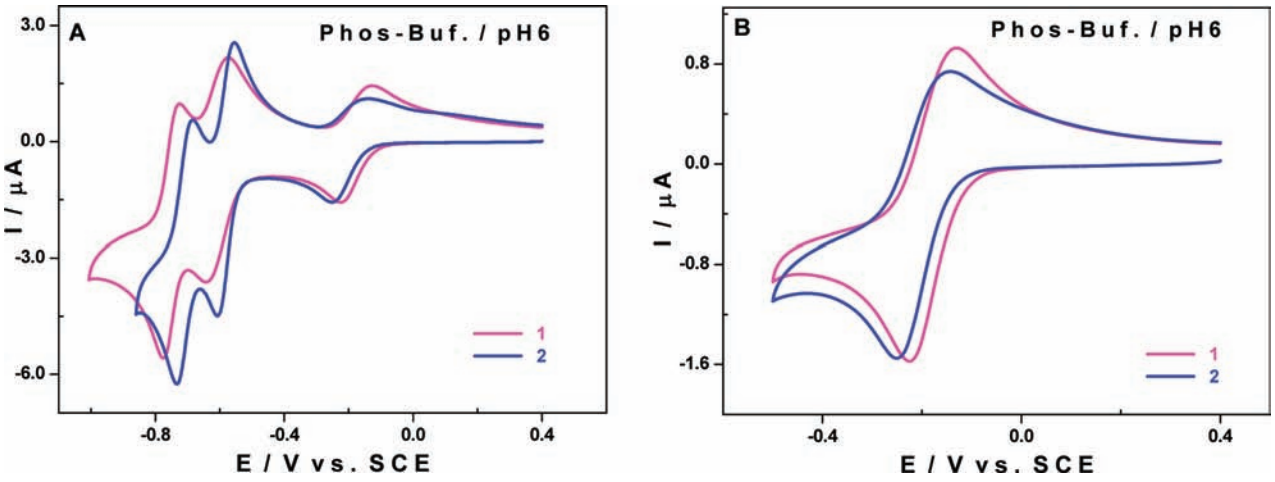

Figure 8. Comparison between cyclic voltammograms of **1** (red line) and **2** (blue line) at pH 6 (0.4 M NaH_2PO_4 + 0.2 M Na_2HPO_4 + H_3PO_4) values. Polyoxometalate concentration, 0.5 mM; scan rate, 10 mV s^{-1}; working electrode, glassy carbon; reference electrode, SCE. (A) Potential scan is extended down to the furthest W waves (−1.15 V vs SCE for both isomers). (B) Potential scan is restricted to the Fe wave (−0.50 V vs SCE for both isomers).

HPO_4^{2-}, which is a very weak acid. Definitely, the $E_{pc}(Fe^{3+})_1$ shift is so narrow that at pH 6.00 we observe what can be referred to as an inversion of peak potential values; $E_{pc}(Fe^{3+})_2$ is now lower than $E_{pc}(Fe^{3+})_1$ (Figure 8).

Below pH 6, $(Fe^{3+})_2$ is easier to reduce than $(Fe^{3+})_1$, i.e., $E_{pc}(Fe^{3+})_2 > E_{pc}(Fe^{3+})_1$ (Figure 9, Table 4). This is an

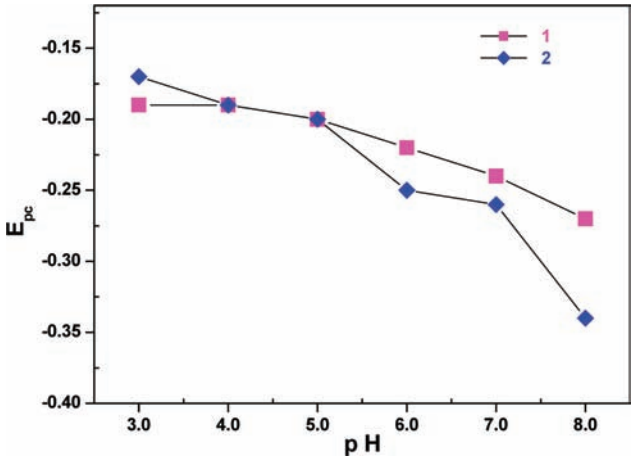

Figure 9. Evolution of peak reduction potential values, $E_{pc}(Fe^{3+/2+})$, as a function of pH for **1** (red square) and **2** (blue diamond). CVs are recorded at a scan rate of 10 mV s^{-1} on a glassy carbon working electrode. Potentials are quoted against the SCE reference electrode.

unexpected behavior since all theoretical and experimental studies performed on this family of compounds (plenary Wells−Dawson structures, $X_2W_{18}O_{62}^{6-}$ X = As or P, and monosubstituted complexes, α_1- and α_2-$X_2MW_{17}O_{62}^{n-}$, M = Mo, Tc, V, Re), pointed out that the first electronic exchange preferentially takes place on one of the 12 W atoms located in the equatorial region of the molecule, i.e., the α_1 position.[16−21,24−29] In other words, the α_1 isomer should always be easier to reduce than the corresponding α_2 isomer. However, this accepted and demonstrated rule is, in the case of α_1 and α_2 $P_2W_{17}Fe$ isomers, up-to-default. Indeed, we report here that the influence of the protonation makes a difference in the electrochemical behavior of both isomers, making the reduction

Table 4. Peak Reduction Potential Values, E_{pc}, for Fe^{3+} Redox Process and First Three W^{6+} Redox Processes for 1 and 2 in 0.4 M NaH_2PO_4 + 0.2M Na_2HPO_4 + H_3PO_4 in the Range of pH 3 to 8[a]

		E_{pc} ($Fe^{3+/2+}$)	E_{pc} (W_1)	E_{pc} (W_2)	E_{pc} (W_3)
1	pH 3	−0.19	−0.45	−0.54	−0.89
	pH 4	−0.19	−0.55	−0.64	−0.97
	pH 5	−0.20	−0.60	−0.71	−1.03
	pH 6	−0.22	−0.64	−0.77	−1.09
	pH 7	−0.24	−0.68	−0.87	−1.16
	pH 8	−0.27	−0.71	−1.04	−1.25
2	pH 3	−0.17	−0.37	−0.51	−0.77; −0.88
	pH 4	−0.19	−0.49	−0.55	−0.83; −0.92
	pH 5	−0.20	−0.54	−0.66	−0.93
	pH 6	−0.25	−0.61	−0.73	−0.97
	pH 7	−0.26	−0.66	−0.82	−0.97; −1.04
	pH 8	−0.34	−0.74	−0.98	−1.10

[a]Potentials are quoted against SCE reference electrode. Scan rate, 10 mV·s^{-1}; working electrode, glassy carbon.

of the Fe center in the α_2 position easier than in the case of the α_1 isomer. In contrast, when the protonation effect becomes negligible (for pH equal or higher than 6 or in organic medium), the normal trend is recovered; i.e., the Fe center in the α_1 position is easier to reduce than Fe center in the α_2 position.

4. Influence of Buffer Composition for a Given pH. When dissolved in an electrolyte with a buffer capacity {pk_a (AH/A^-)}, the POM-based molecule undergoes a protonation reaction that can be summarized as follows:

$$AH \rightleftharpoons A^- + H^+ \quad (7)$$

$$POM + H^+ \rightleftharpoons POMH^+ \quad (8)$$

Therefore, it seems clear that the degree of protonation of the POM molecule will depend on the degree of dissociation of the acid form of the buffer. The better the buffer is dissociated, the greater will be the protonation of the POM and the easier will be its reduction. In other words, at a given pH for the same electrolyte, the protonation will increase with the ratio [A^-]/[AH] and will make the reduction process easier (E_{pc} less

dx.doi.org/10.1021/ic300090f | Inorg. Chem. 2012, 51, 6129−6138

negative). This behavior is well-illustrated in Figure 10, below which present CVs of **2** at pH 4 in three different medium

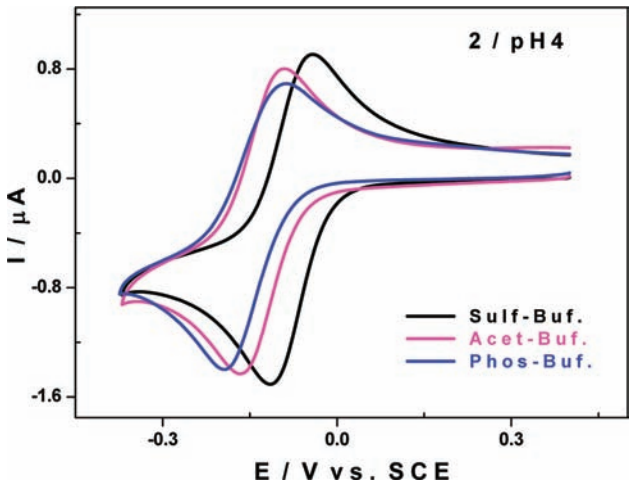

Figure 10. Comparison of cyclic voltammograms of **2** at pH 4 in different buffer solutions. Sulfate buffer (black line), acetate buffer (red line), and phosphate buffer (blue line). Polyoxometalate concentration, 0.5 mM; scan rate, 10 mV s^{-1}; working electrode, glassy carbon; reference electrode, SCE. Potential scan is restricted to the Fe wave (−0.37 V vs SCE for both isomers).

(acetate, phosphate, and sulfate). At this pH value, HSO_4^- is completely dissociated (see Table 5, $[SO_4^{2-}]/[HSO_4^-] \approx$

Table 5. Effect of the Acid−Base Properties of the Electrolyte on the Redox Potential for Fe within 2 at pH 4 and pH 6[a]

	SO_4^{2-}/ HSO_4^-	CH_3COO^-/ CH_3COOH	HPO_4^{2-}/ $H_2PO_4^-$	
$[A^-]/[AH]$	1.26×10^2	2.0×10^{-1}	6.3×10^{-4}	pH 4
E_{pc}	−0.11	−0.17	−0.19	
$[A^-]/[AH]$		2.0×10^1	6.3×10^{-2}	pH 6
E_{pc}		−0.17	−0.25	

[a] A^- = SO_4^{2-}, CH_3COO^-, HPO_4^{2-}; AH = HSO_4^-, CH_3COOH, $H_2PO_4^-$.

126); we can therefore consider that **2** is in its highest degree of protonation. As expected, the reduction of **2** is easier in this medium (E_{pc} = −0.11 V) than in acetate or phosphate buffers (E_{pc} = −0.17 V and −0.19 V, respectively), which are less dissociated at pH 4 ($[CH_3COO^-]/[CH_3COOH] \approx 0.2$; $HPO_4^{2-}/H_2PO_4^- \approx 6.3 \times 10^{-4}$). This effect is less evident with **1**. In fact, as described above and discussed in the DFT calculation section, pH and protonation effects are less pronounced when the substitution is at the alpha1 position instead of alpha 2.

DFT Calculations. To complement the electrochemical results, density functional based calculations have been performed to help explain the relative stability and redox potentials of the iron-substituted Dawson anions **1** and **2** and their dependence with protonation. The acidity of the solution has been revealed to be determinant in the evolution of the redox properties of both isomers. Since we are not capable of explicitly imposing a given pH value to our standard DFT calculations, we have generated a number of differently protonated model structures derived from the parent $[P_2W_{17}FeO_{62}]^{6-}$ that are assumed to be dominant at different pH values. Namely, at neutral pH, the deprotonated $[FeOP_2W_{17}O_{61}]$ structure could be predominant. However, this is not expected regarding the experimental evidence that rules out the stability of these molecules.[30] Another likely structure at neutral pH is the monoprotonated one, $[Fe(OH)P_2W_{17}O_{61}]$. The next protonation step will occur when acidity increases to pH 5, obtaining $[Fe(OH_2)P_2W_{17}O_{61}]$. Finally, at even lower pH, another two structures could be formed. The first one is the structure with no terminal atom on the Fe site $[FeP_2W_{17}O_{61}]$, and the second one is the structure with a water molecule linked to the iron atom and a protonated bridging oxygen, $[HFe(OH_2)P_2W_{17}O_{61}]$.

We have obtained fully optimized structures for this set of systems with Fe^{2+} and Fe^{3+} and evaluated the reduction free energy,[36] ΔG_1 and ΔG_2, for the two isomers. We have also extracted the reduction free energy differences ($-\Delta\Delta G_{2\text{-}1} = -\Delta G_2 + \Delta G_1$) to compare them with the experimental data ($\Delta E_{1/2}{}^0$; see Table 6). If the monoprotonated $Fe^{III}(OH)$

Table 6. Computed Reduction Energies for Differently Protonated Forms of Isomers 1 and 2 (ΔG_i, in eV), Reduction Energy Differences ($-\Delta\Delta G_{2-1}$), and Experimental Data ($\Delta E_{1/2}{}^0$, in V)

	ΔG_1	ΔG_2	$-\Delta\Delta G_{2-1}$	$\Delta E_{1/2}{}^0$ (exptl.)
$[Fe(OH)P_2W_{17}O_{61}]^{8-}$	−4.017	−4.000	−0.017	−0.030
$[Fe(OH_2)P_2W_{17}O_{61}]^{7-}$	−4.592	−4.639	+0.047	+0.080
$[FeP_2W_{17}O_{61}]^{7-}$	−4.746	−4.814	+0.068	
$[HFe(OH_2)P_2W_{17}O_{61}]^{6-}$	−4.853	−4.943	+0.090	

species are considered, the reduction occurs more easily for **1**; that is, its reduction energy is more negative than for **2** by 17 meV, in good agreement with the experimental half-wave potentials ($\Delta E_{1/2}{}^0$ = +30 mV). The trend is inverted by adding the second proton to the iron-substituted species (simulated moderately acidic pH), when $-\Delta\Delta G_{2-1}$ = 47 meV. Under conditions of further protonation (pH 1), this trend is more notable, and $-\Delta\Delta G_{2-1}$ rises to 68 or 90 meV, depending on the model, in favor of **2**. Our calculations reproduce the trend observed in the experiments.

We would like to point out that three different species, $[Fe(OH_2)P_2W_{17}O_{61}]$, $[FeP_2W_{17}O_{61}]$, and $[HFe(OH_2)P_2W_{17}O_{61}]$ can be formed as the acidity increases. There is neither experimental nor theoretical evidence that suggests which one is predominant, or if a mixture of them coexists in solution. Nevertheless, all of them feature the same redox behavior in good agreement with the experimental data (Table 6).

The uncommon feature that isomers **1** and **2** reverse the ordering of their first reduction potentials at pH 6 deserves further insight. From the electrochemical experiments, we observed that the first 1e-reduction takes place at the Fe center irrespective of the isomer and the pH, to the detriment of the formation of the blue species, $P_2W_{17}Fe^{3+} \rightarrow [P_2W_{17}Fe^{3+}$ 1e], a process that takes place at more negative potentials. So, the delocalized d_{xy}-like molecular orbital of W character appearing at higher energies, also of nonbonding nature, can be ruled out of the competition toward the first incoming electron. From our DFT results, the orbitals of the oxidized forms of **1** and **2** ready to accept an extra electron are, in principle, the formally nonbonding d_{xy}(Fe) (perpendicular to the terminal oxygen) and the antibonding π^*(Fe−O), which is oriented toward the

dx.doi.org/10.1021/ic300090f | Inorg. Chem. 2012, 51, 6129−6138

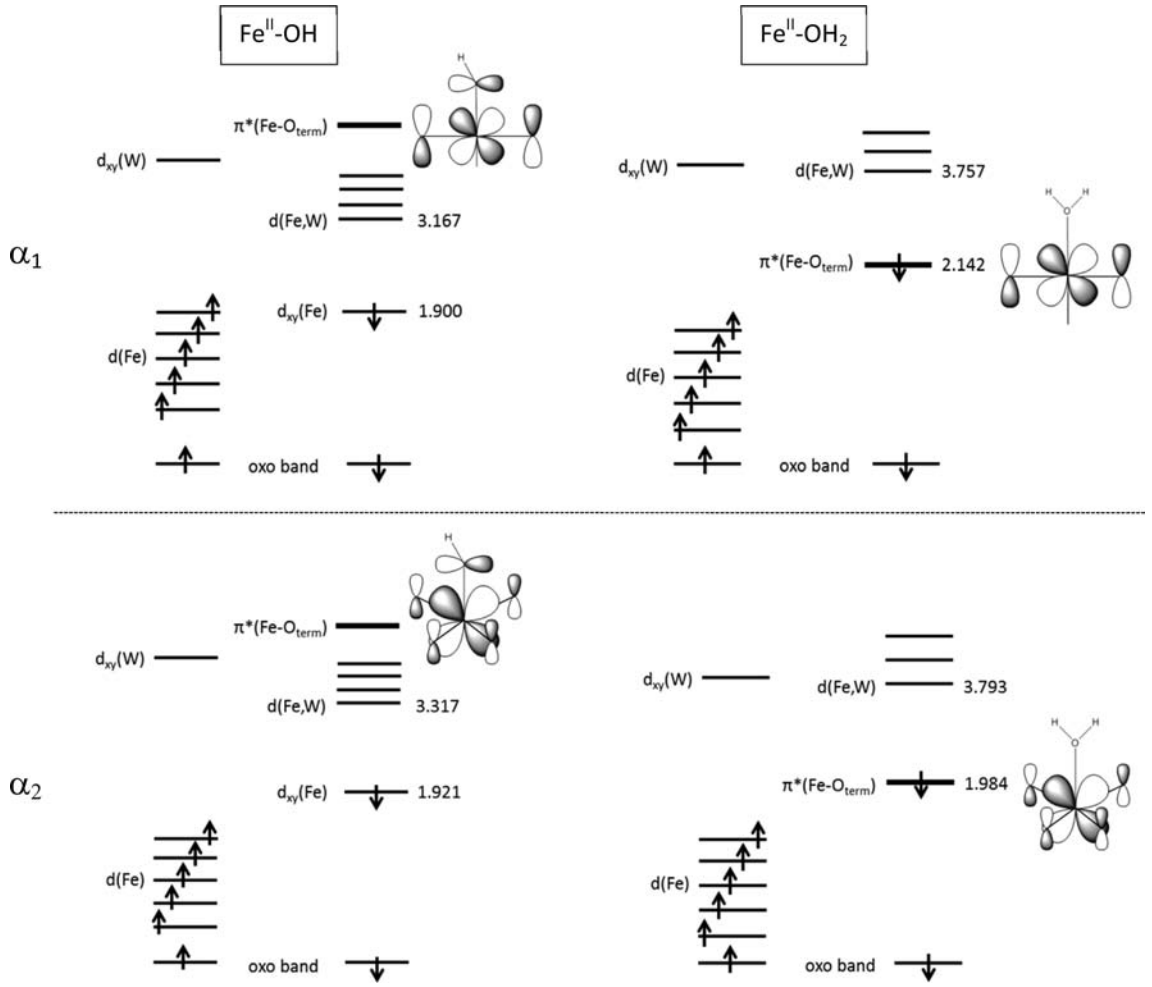

Figure 11. Computed frontier orbitals for the $Fe^{II}(OH)$ and $Fe^{II}(OH_2)$ forms of **1** and **2**. The character and relative energies (in eV vs the highest orbital of the oxo band) are shown for some molecular orbitals. Spin-up and spin-down orbitals are separated in two columns for each compound.

terminal oxygen. The energy of the latter orbital strongly depends on the Fe−O(terminal) mutual interaction, which, in addition, is changing with pH. In both Fe^{2+} isomers, the d_{xy} orbital is more stable than the π^* orbital under conditions of poor protonation ($FeOP_2W_{17}O_{61}$ and $Fe(OH)P_2W_{17}O_{61}$ structures) while the inversion occurs for $[FeP_2W_{17}O_{61}]$ and $[Fe(OH_2)P_2W_{17}O_{61}]$ molecules, assumed to be the predominant species at low pH. This is not so evident for both isomers of the Fe^{3+} form, where the orbital reversal occurs for the α_2 isomer only. This particular behavior depending on pH is not observed in other metal-substituted Dawson-type tungstodiphosphates, such as $P_2W_{17}M$ with M = V or Mo.[24−29]

We demonstrate below that the antibonding Fe−O(terminal) interaction changes depending on the pH conditions, namely, the protonation state of the system, and governs the inversion of the order in reduction potentials observed around pH 5 for **1** and **2**. As expected, the computed Fe−O(terminal) distance increases with the number of protons attached to the terminal oxygen. Under conditions of no protonation at Fe−O, the computed distance is d(Fe−O) ∼ 1.66−1.76 Å depending on the isomeric form, with the π^*(Fe−O) orbital lying at high energies with respect to the d_{xy}(Fe) one due to its marked antibonding nature. The general evolution of the π^*(Fe−O) orbital from neutral to acidic pH is depicted in Figure 11, showing the differences in the molecular orbital sequence for the mono- and diprotonated forms of **1** and **2**. For the monoprotonated species, $Fe^{III}(OH)$, the Fe−O distance increases to ∼1.87 Å and the π^*(Fe−O) is stabilized due to the lower participation of the 2p-O(terminal) orbital but still remains located above the d_{xy}-Fe orbital. Finally, when the apical group is doubly protonated, $Fe^{III}(OH_2)$, the Fe−O distance becomes very long (2.08 Å) and the π^*(Fe−O) orbital turns into a "pure" d_{xz}-Fe orbital, more stable than the formally nonbonding d_{xy}(Fe) orbital when an extra electron is added.

The more favorable reduction of **2** at pH ≤ 5 compared to **1** can be explained by (i) the dominant role of the $\pi^*(Fe-OH_2)$ orbital in the reduction process and (ii) the different orientation of this orbital in either isomeric form with respect to the bridging oxygen atoms surrounding the iron center. The right-hand part of Figure 11 shows that the orientation of the π^* orbital in **1** coincides with the direction of two Fe−O(bridging) bonds, therefore conferring a stronger antibonding character than the homologous orbital in **2**. In the latter case, the π^* orbital bisects the Fe−O(bridging) bonds, making the 3d(Fe)−2p(O) interaction weaker. Thus, electron reduction takes place in a higher π^* orbital in the **1** isomer than in **2** and makes the reduction of the latter compound more favorable at sufficiently acidic pH.

A quantitative approach by atomic spin population analysis confirms the above statements. The computed change in spin density of O(terminal) on going from Fe−OH to $Fe-OH_2$ is remarkable: 0.36 to 0.06 for both α_1 and α_2 forms of $P_2W_{17}Fe^{III}$.

dx.doi.org/10.1021/ic300090f | Inorg. Chem. 2012, 51, 6129−6138

This indicates the decreasing participation of the terminal oxygen in the π^*(Fe−O) orbital. For the reduced $P_2W_{17}Fe^{II}$ compounds, the spin density changes from 0.16 to 0.02 on average for both isomers. The smaller spin density values in the case of reduced forms arise from the longer Fe−O(terminal) distances produced by the population of the π^*(Fe−O) orbital. In summary, protonation on the terminal Fe−O site gradually stabilizes the π^* orbital with respect to the d_{xy} one, leading to an inversion of the d_{xy} and π^* (d_{xz}-Fe) orbital energies when the apical group of iron is water. Calculations have revealed that this occurs in both isomeric forms (see Figure SI-17).

CONCLUSIONS

Reinvestigation of the redox properties of **1** and **2** confirms that, at low pH values (pH ≤ 5), the reduction of the Fe center in the α_2 position is easier than in the α_1 position. This behavior can be related to the influence of the protonation. Indeed, at higher pH values (pH ≥ 6) or in an organic medium, when the protonation effect becomes negligible, the normal trend is recovered; i.e., the reduction of the Fe center in the α_1 position becomes easier than in the α_2 position as expected. We also described the influence of the electrolyte pk_a (in the case of aqueous buffer solutions) at a given pH value.

The computational study performed on both α_1- and α_2-$P_2W_{17}Fe$ isomers explains their electrochemical behavior. We were able to interpret the experimental results according to the different molecular orbital energies. We have also evidenced the influence of the protonation state of the iron derivative on the relative reduction potentials of both isomers. At pH values close to 6, reduction energies are more favorable to α_1, while the opposite trend is observed at low pH values due to the double protonation at the terminal Fe−O site. In both Fe^{II} isomers, the d_{xy} orbital is more stable than the π^* orbital for [Fe(OH)-$P_2W_{17}O_{61}$], assumed to be dominant at neutral pH, while the inversion occurs for [$Fe(OH_2)P_2W_{17}O_{61}$] and [$FeP_2W_{17}O_{61}$], the principal species at low pH.

ASSOCIATED CONTENT

Supporting Information

Additional experimental data and DFT calculations data (figures and tables). This material is available free of charge via the Internet at http://pubs.acs.org.

AUTHOR INFORMATION

Corresponding Author

*Tel.: +34977558283 (X.L.), +33139254419 (I.M.M.). Fax +34977559563 (X.L.), +33139254419 (I.M.M.). E-mail: javier.lopez@urv.cat (X.L.), israel.mbomekalle@chimie.uvsq.fr (I.M.M.).

Notes

The authors declare no competing financial interest.

ACKNOWLEDGMENTS

This work was supported by the Centre National de la Recherche Scientifique CNRS (UMR 8180), the University of Versailles and by the Spanish MICINN (CTQ2011-29054-C02-01), the Generalitat de Catalunya (2009SGR-00462), and the XRQTC. X.L. thanks the Ramón y Cajal program (grant no. RYC-2008-02493).

REFERENCES

(1) Souchay, P.; Hervé, G. *C. R. Acad. Sci.* **1965**, *261*, 2486−2489.
(2) Souchay, P.; Contant, R. *C. R. Acad. Sci.* **1967**, *265*, 723−726.
(3) Massart, R.; Hervé, G. *Rev. Chim. Miner.* **1968**, *5*, 501−520.
(4) Fruchart, J.-M.; Hervé, G. *Ann. Chim.* **1971**, *6*, 337−348.
(5) Pope, M. T.; Varga, G. M., Jr. *Inorg. Chem.* **1966**, *5*, 1249−1257.
(6) Pope, M. T.; Papaconstantinou, E. *Inorg. Chem.* **1967**, *6*, 1147−1152.
(7) Papaconstantinou, E.; Pope, M. T. *Inorg. Chem.* **1967**, *6*, 1152−1155.
(8) Varga, G. M., Jr.; Papaconstantinou, E.; Pope, M. T. *Inorg. Chem.* **1970**, *9*, 662−667.
(9) Papaconstantinou, E.; Pope, M. T. *Inorg. Chem.* **1970**, *9*, 667−669.
(10) Weinstock, I. A. *Chem. Rev.* **1998**, *98*, 113−170.
(11) Sadakane, M.; Steckhan, E. *Chem. Rev.* **1998**, *98*, 219−237.
(12) Keita, B.; Nadjo, L. Electrochemistry of Isopoly and Heteropoly Oxometalates. *Encyclopedia of Electrochemistry*; Bard, A. J., Stratmann, M., Eds.; Wiley-VCH: Weinheim, Germany, 2007; Vol 7, pp 607−700.
(13) Keita, B.; Nadjo, L. Electrochemical Reactions on Modified Electrodes. *Encyclopedia of Electrochemistry*; Bard, A. J., Stratmann, M., Eds.; Wiley-VCH: Weinheim, Germany, 2007; Vol *10*, pp 685−728.
(14) Keita, B.; Nadjo, L.; Savéant, J.-M. *J. Electroanal. Chem.* **1988**, *243*, 105−116.
(15) Prenzler, P. D.; Boskovic, C.; Bond, A. M.; Webb, A. G. *Anal. Chem.* **1999**, *71*, 3650−3656.
(16) Keita, B.; Jean, Y.; Levy, B.; Nadjo, L.; Contant, R. *New J. Chem.* **2002**, *26*, 1314−2319.
(17) López, X.; Bo, C.; Poblet, J. M. *J. Am. Chem. Soc.* **2002**, *124*, 12574−12582.
(18) Fernández, J. A.; López, X.; Bo, C.; de Graaf, C.; Baerends, E. J.; Poblet, J. M. *J. Am. Chem. Soc.* **2007**, *129*, 12244−12253.
(19) Yan, L.; López, X.; Carbó, J. J.; Sniatynsky, R. T.; Duncan, D. D.; Poblet, J. M. *J. Am. Chem. Soc.* **2008**, *130*, 8223−8233.
(20) de Graaf, C.; López, X.; Ramos, J. L.; Poblet, J. M. *Phys. Chem. Chem. Phys.* **2010**, *12*, 2716−2721.
(21) El Moll, H.; Nohra, B.; Mialane, P.; Marrot, J.; Dupré, N.; Riflade, B.; Malacria, M.; Thorimbert, S.; Hasenknopf, B.; Lacôte, E.; Aparicio, P. A.; López, X.; Poblet, J. M.; Dolbecq, A. *Chem.—Eur. J.* **2011**, *17*, 14129−14138.
(22) Mbomekallé, I.-M.; López, X.; Poblet, J. M.; Sécheresse, F.; Keita, B.; Nadjo, L. *Inorg. Chem.* **2010**, *49*, 7001−7006.
(23) Keita, B.; Belhouari, A.; Nadjo, L.; Contant, R. *J. Electroanal. Chem.* **1998**, *442*, 49−57.
(24) Contant, R.; Ciabrini, J. P. *J. Chem. Res., Synop.* **1977**, 222, *J. Chem. Res. Miniprint* 2601.
(25) Acerete, R.; Harmalker, S.; Hammer, C. F.; Pope, M. T.; Baker, L. C. W. *J. Chem. Soc., Chem. Commun.* **1979**, 777−779.
(26) Ciabrini, J. P.; Contant, R.; Fruchart, J. M. *Polyhedron* **1983**, *2*, 1229−1233.
(27) Harmalker, S. P.; Leparulo, M. A.; Pope, M. T. *J. Am. Chem. Soc.* **1983**, *105*, 4286−4292.
(28) Abbessi, M.; Contant, R.; Thouvenot, R.; Hervé, G. *Inorg. Chem.* **1991**, *30*, 1695−1702.
(29) Keita, B.; Mbomekalle, I. M.; Nadjo, L.; de Oliveira, P.; Ranjbari, A.; Contant, R. *C. R. Chim.* **2005**, *8*, 1057−1066.
(30) Contant, R.; Abbessi, M.; Canny, J.; Belhouari, A.; Keita, B.; Nadjo, L. *Inorg. Chem.* **1997**, *36*, 4961−4967.
(31) Keita, B.; Nadjo, L. *J. Electroan. Chem.* **1987**, *217*, 287−304.
(32) Frisch, M. J.; Trucks, G. W.; Schlegel, H. B.; Scuseria, G. E.; Robb, M. A.; Cheeseman, J. R.; Scalmani, G.; Barone, V.; Mennucci, B.; Petersson, G. A.; Nakatsuji, H. C., M.; Li, X.; Hratchian, H. P.; Izmaylov, A. F.; Bloino, J.; Zheng, G.; Sonnenberg, J. L.; Hada, M.; Ehara, M.; Toyota, K.; Fukuda, R.; Hasegawa, J.; Ishida, M.; Nakajima, T.; Honda, Y.; Kitao, O.; Nakai, H.; Vreven, T.; Montgomery, J. A., Jr.; Peralta, J. E.; Ogliaro, F.; Bearpark, M.; Heyd, J. J.; Brothers, E.; Kudin, K. N.; Staroverov, V. N.; Kobayashi, R.; Normand, J.; Raghavachari, K.; Rendell, A.; Burant, J. C.; Iyengar, S. S.; Tomasi, J.; Cossi, M.; Rega, N.; Millam, N. J.; Klene, M.; Knox, J. E.; Cross, J. B.; Bakken, V.; Adamo, C.; Jaramillo, J.; Gomperts, R.; Stratmann, R. E.; Yazyev, O.; Austin, A. J.; Cammi, R.; Pomelli, C.; Ochterski, J. W.; Martin, R. L.;

Morokuma, K.; Zakrzewski, V. G.; Voth, G. A.; Salvador, P.; Dannenberg, J. J.; Dapprich, S.; Daniels, A. D.; Farkas, Ö.; Foresman, J. B.; Ortiz, J. V.; Cioslowski, J.; Fox, D. J. *Gaussian 09*, revision A.1; Gaussian, Inc.: Wallingford, CT, 2009.
(33) Lee, C. T.; Yang, W. T.; Parr, R. G. *Phys. Rev. B* **1988**, *37*, 785−789.
(34) Hay, P. J.; Wadt, W. R. *J. Chem. Phys.* **1985**, *82*, 270−283.
(35) Miertus, S.; Scrocco, E.; Tomasi, J. *Chem. Phys.* **1981**, *55*, 117−129.
(36) We only consider the electronic contribution to the free energy, $G = E$. The entropic term is assumed to be much smaller, not affecting the values discussed.